Inorg. Chem. **2009**, *48*, 3198−3204

Single Crystal Electron Paramagnetic Resonance Spectra of Cs_2MnF_6 and K_2MnF_6 Diluted in the Isomorphous Germanium Salts

Christian Aagaard Thuesen,[†] Anne-Laure Barra,[‡] and Jørgen Glerup*,[†]

Department of Chemistry, University of Copenhagen, Universitetsparken 5, København Ø, DK 2100 Denmark, and Grenoble High Magnetic Field Laboratory−CNRS, 25 Avenue des Martyrs, 38042 Grenoble Cedex 9, France

Received November 20, 2008

In this work single crystal electron paramagnetic resonance (EPR) spectra of Cs_2MnF_6 and K_2MnF_6 diluted in the similar germanium salts have been interpreted and fitted. The spectra of the cubic cesium salt were recorded with the magnetic field parallel with the 4-fold axis and with the 3-fold axis. The spectrum along the 4-fold axis looks as expected with six groups from the manganese nuclear spin each split into seven lines caused by the nuclear spin from the six fluorine ligands. The spectrum along the 3-fold axis contains considerably more lines. This can be explained by the fact that only the transitions with the M_S values $-1/2 \leftrightarrow 1/2$ are observed together with the fact that the nuclear Zeeman effect from the six fluorine ligands mixes states and makes forbidden transitions allowed. The spectra of the trigonal potassium salt are recorded along the 3-fold axis and perpendicular to this axis. The sign of the zfs parameter was determined by high frequency EPR spectroscopy at low temperature. The knowledge of this meant that we could determine the sign of the two fluorine hyperfine coupling parameters both in this case and in the cubic case.

Introduction

Ever since the early days of electron paramagnetic resonance (EPR), superhyperfine interaction, that is, the interaction between the electron spin on the metal and the nuclear spin on the ligands, has been used to elucidate the covalency of the metal ligand bonds.[1,2] Especially the fluoride ligand has attracted attention, partly because many complexes of the metals from the first transition series can be prepared and partly because fluoride is a strong π-donor.[3] Furthermore, the interaction with fluorine is more pronounced because of the big value for the nuclear *g*-factor. However, whereas most of such measurements have been conducted among the ions with an orbitally non-degenerate ground state, only one short investigation has been made for Mn(IV).[4]

Because of the exceedingly big matrix dimensions resulting from the nuclear spins of the fluoride ligands, the interpretation of most hexafluoride spectra has rested on approximate methods utilizing perturbation theory taken to various orders to account for both the fluorine superhyperfine interaction and the nuclear Zeeman effect.

In the past we have successfully extracted EPR parameters from powder spectra.[5−8] However, the matrix size and the number of transitions forced us to work with single crystals. We herein report a detailed investigation of single crystal EPR spectra of hexafluoromanganate(IV) diluted in the diamagnetic hosts Cs_2GeF_6 and K_2GeF_6. The hosts are strictly cubic and trigonal distorted, respectively. The cubic cesium compounds Cs_2GeF_6 and Cs_2MnF_6 belong to the same space group and have almost equal bond lengths.[9,10] The same is the case for the hexagonal potassium salts, yet, whereas

* To whom correspondence should be addressed. E-mail: glerup@kiku.dk.
† University of Copenhagen.
‡ Grenoble High Magnetic Field Laboratory−CNRS.

(1) Owen, J.; Stevens, K. W. H. *Nature* **1953**, *171*, 836–836.
(2) Owen, J.; Thornley, J. H. M. *Rep. Prog. Phys.* **1966**, *29*, 675–728.
(3) Glerup, J.; Mønsted, O.; Schäffer, C. E. *Inorg. Chem.* **1976**, *15*, 1399–1407.
(4) Helmholz, L.; Guzzo, A. V.; Sanders, R. N. *J. Chem. Phys.* **1961**, *35*, 1349–1352.
(5) Glerup, J.; Goodson, P. A.; Hodgson, D. J.; Masood, M. A.; Michelsen, K. *Inorg. Chim. Acta* **2005**, *358*, 295–302.
(6) Glerup, J.; Larsen, S.; Weihe, H. *Acta Chem. Scand.* **1993**, *47*, 1154–1161.
(7) Glerup, J.; Weihe, H. *Inorg. Chem.* **1997**, *36*, 2816–2819.
(8) Sanzenbacher, R.; Böttcher, A.; Elias, H.; Hüber, M.; Haase, W.; Glerup, J.; Jensen, T. B.; Neuburger, M.; Zehnder, M.; Springborg, J.; Olsen, C. E. *Inorg. Chem.* **1996**, *35*, 7493–7499.
(9) Hoppe, R.; Hofmann, B. *Z. Anorg. Allg. Chem.* **1977**, *436*, 65–74.
(10) Schütz, W. *Z. Phys. Chem. B* **1936**, *36*, 292–308.

10.1021/ic802223j CCC: $40.75
Published on Web 03/05/2009

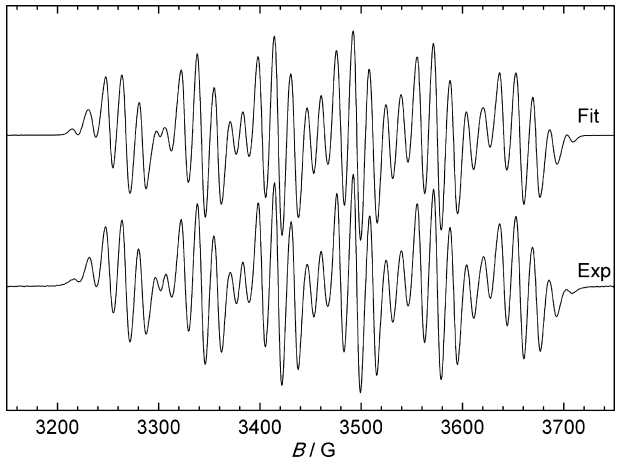

Figure 1. EPR spectrum of diluted Cs_2MnF_6 single crystal recorded along the 4-fold axis at 25 K, $\nu = 9.6396$ GHz.

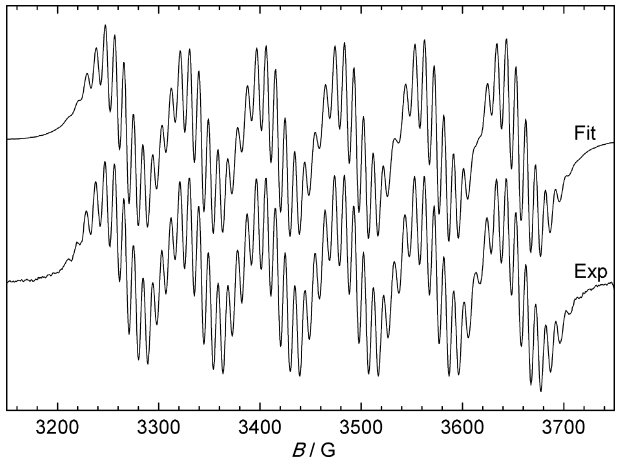

Figure 2. EPR spectrum of diluted Cs_2MnF_6 single crystal recorded along the 3-fold axis at 25 K, $\nu = 9.6396$ GHz.

K_2GeF_6 is trigonally compressed to a different extent on each side of the germanium ion, K_2MnF_6 is trigonally compressed on one side and elongated on the other.[11,12] Both trigonally distorted compounds therefore have two sets of slightly different fluoride ligands.

The pronounced fluoride superhyperfine interaction leads to a comprehensive splitting pattern which may serve as a good textbook example. All fitted and simulated spectra have been calculated through complete diagonalization of the full energy matrix.

Experimental Section

The X-band spectra were recorded on a Bruker Elexsys E 500 spectrometer equipped with a dual mode cavity ER 4116DM, a programmable goniometer ER 218G1, ER 035 M NMR-Gaussmeter, and an EIP 538B frequency counter. The system was cooled with an Oxford Instruments cryostat ESR-900 controlled by an Oxford Instruments ITC 503 temperature unit. The magnetic field

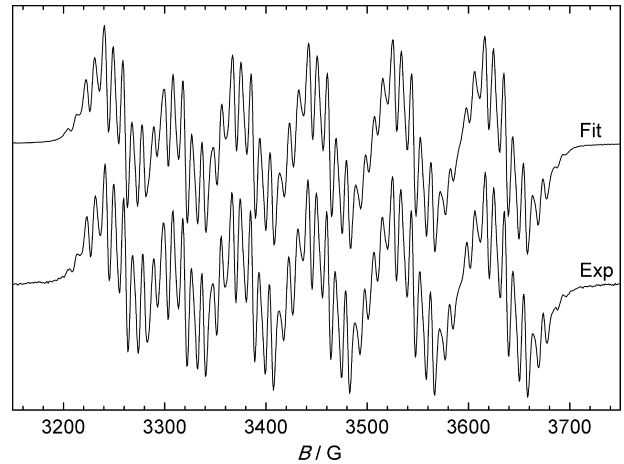

Figure 3. EPR spectrum showing the transition $-1/2 \leftrightarrow 1/2$ in diluted K_2MnF_6 recorded along the 3-fold axis (cf. Figure 8A), $\nu = 9.6370$ GHz.

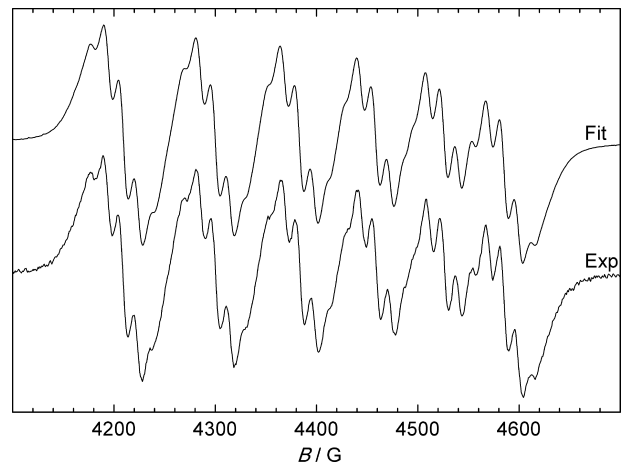

Figure 4. EPR spectrum showing the transition $3/2 \leftrightarrow 1/2$ in diluted K_2MnF_6 recorded along the 3-fold axis (cf. Figure 8B), $\nu = 9.6370$ GHz.

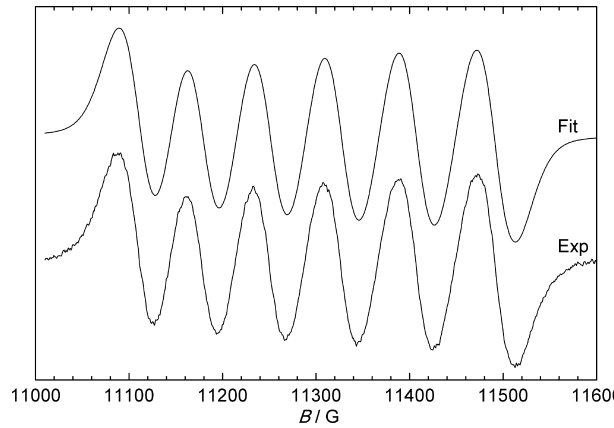

Figure 5. EPR spectrum showing the transition $1/2 \leftrightarrow 3/2$ in diluted K_2MnF_6 recorded along the 3-fold axis (cf. Figure 8C), $\nu = 9.6370$ GHz.

was calibrated with the NMR-Gaussmeter which gives six digits which together with the six digits from the frequency counter determines the accuracy.

Warning! *Because of its highly skin corrosive nature hydrofluoric acid should be treated with great care.*

By chance two different approaches were utilized in synthesizing the single crystals of M_2MnF_6 diluted in M_2GeF_6 (M = Cs or K). One was to produce Mn(IV) in situ through ethereal reduction of permanganate[13] in a solution of the host. The second approach was

(11) Bode, H.; Brockmann, R. *Z. Anorg. Allg. Chem.* **1952**, *269*, 173–178.
(12) Bukovec, P.; Hoppe, R. *J. Fluorine Chem.* **1983**, *23*, 579–587.
(13) Palmer, W. G. *Experimental Inorganic Chemistry*; University Press: Cambridge, 1959.

first to synthesize and isolate the hexafluoromanganate(IV) salt followed by isolation and dilution in the corresponding germanium salt. Both approaches are described below. It is a mere coincidence which of the syntheses is made with the cesium salt and the potassium salt, respectively. According to Gmelin, organic solvents other than ether cannot be used for the reduction because of a tendency of reducing permanganate to Mn(III).[14]

Because of instability of the Mn(IV) ion in solution, it is crucial that the crystallization takes place in the cold. We were not able to detect any proper Mn(IV) EPR signal in crystals grown at room temperature. This is probably due to degradation into Mn(III). The use of 40% hydrofluoric acid in one synthesis and 48% in another was tried to minimize Mn(IV) degradation. This was before realizing that cooling was the main key to a successful synthesis. A quick way of checking the presence of Mn(IV) in the host crystals is placing them under ultraviolet light where they glow with an intense red color owing to the Mn(IV) $^2E_g \rightarrow {}^4A_{2g}$ phosphorescence transition.

To speed up solvent evaporation and thereby further minimizing degradation, the crystals were grown in an evacuated polycarbonate desiccator. An evaporation speed of about 4 mL solvent per day produced EPR suitable single crystals.

Single Crystals of Cs_2MnF_6 in Cs_2GeF_6. In a plastic beaker fitted with magnetic stirring 0.52 g (5.00 mmole) of GeO_2 is dissolved in about 30 mL of 40% hydrofluoric acid. Afterward 1.75 g (5.37 mmole) of Cs_2CO_3 is slowly added as is 56.3 mg (356 μmole) of firmly ground $KMnO_4$. With a Hamilton syringe a drop of diethyl ether is added every 15 min until only a faint purple color remains (about 4 drops). The beaker is placed in a polycarbonate desiccator fitted with concentrated sulfuric acid and solid NaOH. After evacuation the desiccator is stored at 5 °C. Within a few days millimeter big octahedral single crystals are obtained. The crystals are suction dried with plastic equipment.

Single Crystals of K_2MnF_6 in K_2GeF_6. In a plastic beaker 1.00 g (3.78 mmole) of K_2GeF_6 (prepared by evaporating a solution of stoichiometric amounts of GeO_2 and KHF_2 in 40% hydrofluoric acid) and 10 mg (40 μmole) of yellow K_2MnF_6[13] are dissolved in 20 mL of 48% hydrofluoric acid. The beaker is placed in a polycarbonate desiccator along with concentrated sulfuric acid and solid NaOH. After evacuating the desiccator it is stored at 5 °C. Within a few days hexagonal plates of single crystals are obtained with a diameter up to 6 mm. The crystals are suction dried with plastic equipment.

Results

Visual Interpretation. Figure 1 and 2 show the spectra of Cs_2MnF_6 diluted in Cs_2GeF_6 recorded along the four- and 3-fold axis at 25 K. The spectrum along the 4-fold axis is separated into six groups resulting from the hyperfine coupling to the manganese ion. Each of these hyperfine signals is split into a number of lines owing to the smaller coupling to the fluoride ligands. With the magnetic field directed along the 4-fold axis the two axial ligands couple with a superhyperfine coupling constant $A_{F||}$ whereas the four equatorial fluoride ligands couple with $A_{F\perp}$. Since each hyperfine signal is split into seven equally spaced lines (some are overlapping with the neighboring groups) with an intensity relationship given by Pascal's triangle for six equivalent fluoride ligands the numerical size of $A_{F||}$ and $A_{F\perp}$ must be almost equal.

When the magnetic field is directed along the 3-fold axis each of the six fluoride ligands couples equivalently and a seven line pattern is again predicted from simple theory no matter the relationship between $A_{F||}$ and $A_{F\perp}$. Yet, the observed spectrum is much more complex. From Figures 1 and 2 it is evident that the experimental line widths depend on the orientation of the crystal relative to the magnetic field. The individual lines in Figure 1 appear broader than the lines in Figure 2. The unequal intensities of the sextet in Figure 1 is a result of the three M_S transitions $-3/2 \leftrightarrow -1/2$, $-1/2 \leftrightarrow 1/2$, and $1/2 \leftrightarrow 3/2$ having comparable or equal bandwidths. Each of these three transitions is split into 42 hyperfine components. As corresponding hyperfine components do not have exactly the same resonance magnetic field, the lines appear broad. By the same token, the equal intensities of the sextet in Figure 2indicate that the separate lines originate from one M_S transition only, mainly $-1/2 \leftrightarrow 1/2$. The other two transitions are broadened and contribute to the spectrum with the wavy background. More insight into this aspect can be extracted by looking at the trigonal distorted salt of K_2MnF_6 diluted in K_2GeF_6 (vide infra). In the K_2MnF_6 spectrum along the unique axis three allowed transitions ($\Delta M_S = \pm 1$, Figures 3−5 and 8) are observed. Of these, however, only the transition $-1/2 \leftrightarrow 1/2$ shows the complicated splitting pattern. Furthermore, the other transitions in the potassium salt seem to be broadened by some effect. Because of the great similarity between the cubic and trigonal system, it can be concluded that the transitions $\pm 1/2 \leftrightarrow \pm 3/2$ experience so much broadening in the cubic spectra that it renders them unobservable.

Fitting of Cs_2MnF_6. The lines in the cubic spectra could be accounted for by utilizing the following spin Hamiltonian:

$$\hat{H} = g\mu_B \mathbf{B}^T \cdot \hat{\mathbf{S}} + A_{Mn} \hat{\mathbf{S}}^T \cdot \hat{\mathbf{I}}_M + \sum_{i=1}^{6} \hat{\mathbf{S}}^T \cdot \mathbf{A}_{F(i)} \cdot \hat{\mathbf{I}}_{F(i)} - \sum_{i=1}^{6} g_{N,F} \mu_N \mathbf{B}^T \cdot \hat{\mathbf{I}}_{F(i)} - g_{N,Mn} \mu_N \mathbf{B}^T \cdot \hat{\mathbf{I}}_{Mn}$$

The fluoride ligands F(1), F(2), and F(3) are placed on the positive side of the x-, y-, and z-axis, respectively, whereas F(4), F(5), and F(6) are placed on the corresponding negative side. The $\mathbf{A}_{F(i)}$ matrices, representing the axial symmetric superhyperfine coupling between electrons and fluoride ligands, are then given by expressions of the following form:

$$\hat{\mathbf{S}}^T \cdot \mathbf{A}_{F(3)} \cdot \hat{\mathbf{I}}_{F(3)} = [\hat{S}_x \quad \hat{S}_y \quad \hat{S}_z] \cdot \begin{bmatrix} A_{F\perp} & 0 & 0 \\ 0 & A_{F\perp} & 0 \\ 0 & 0 & A_{F||} \end{bmatrix} \cdot \begin{bmatrix} \hat{I}_{F(3)x} \\ \hat{I}_{F(3)y} \\ \hat{I}_{F(3)z} \end{bmatrix}$$

The other superhyperfine matrices are made through proper permutation of $A_{F||}$ and $A_{F\perp}$. The g_N-values in the nuclear Zeeman terms were set equal to tabulated values: $g_{N,Mn} = 1.38748716(4)$ and $g_{N,F} = 5.257736(4)$.[15]

The line width depends on the orientation of the sample. Along the 3-fold axis the transitions M_S $\pm 1/2 \leftrightarrow \pm 3/2$ are so broad that only the $-1/2 \leftrightarrow 1/2$ transition is observable. This

(14) Katscher, H. *Gmelin Handbuch der Anorganischen Chemie - Mangan - Teil C4 - Halogenide*; Springer-Verlag: Berlin, 1977.

Table 1. Spin Hamiltonian Parameters

	orientation	g	D/cm^{-1}	$\sigma_D/10^{-4}$ cm^{-1}	$A_{Mn}/10^{-4}$ cm^{-1}	$A_{F\|\|}/10^{-4}$ cm^{-1}	$A_{F\perp}/10^{-4}$ cm^{-1}
Cs_2MnF_6	$\mathbf{B}\|\|C_4$, $\mathbf{B}\|\|C_3$	1.98808(1)	0	10.8(5)	−72.037(3)	−16.76(3)	13.55(1)
K_2MnF_6	$\mathbf{B}\|\|C_3$	1.99012(1)	−0.364515(3)		−71.075(7)	−12.90(5)	16.05(3)
K_2MnF_6	$\mathbf{B}\perp C_3$	1.98466(1)	−0.36121(2)		−72.679(7)	−13.5(5)	14.9(2)

line broadening can be accounted for by assuming the paramagnetic centers suffer from small random trigonal distortions along the 3-fold axes in the crystal. Because the center of the spectrum does not change with orientation, the zero field splitting D has zero as the mean value with a Gaussian spread σ_D around this value.[16] This will selectively broaden the M_S $\pm 1/2 \leftrightarrow \pm 3/2$ transitions. Modeling this broadening by adding spectra calculated for a range of single ion spin Hamiltonian parameters would be an extremely time-consuming task (vide infra). Instead we retain our initial spin Hamiltonian and model the line width variation by including the spread σ_D when calculating the line width Γ for each transition $k \rightarrow l$

$$\Gamma_{kl} = \Gamma_0 + \sum_j \left(\frac{\partial \Delta_{kl}}{\partial D_j}\right)^2 \sigma_{D_j}^2$$

Δ_{kl} is the energy difference between the two relevant energy levels. Γ_0 is a constant, being the same for all transitions. The partial derivatives express the sensitivity of the energy difference Δ_{kl} with respect to the parameters D_j. The D-spreads σ_D are defined relative to $\mathbf{D}_j$ matrices directed along the 3-fold axes, and their principal axes are therefore non-colinear with the chosen coordinate system. The matrices are obtained through rotation of the coordinate system expressing the well-known zero field splitting matrix directed along the z-axis:

$$\mathbf{D}_j = \mathbf{R}_j \begin{bmatrix} \frac{-D}{3} & 0 & 0 \\ 0 & \frac{-D}{3} & 0 \\ 0 & 0 & \frac{2D}{3} \end{bmatrix} \mathbf{R}_j^{\mathrm{T}}$$

Preliminary attempts to fit the cubic spectra without using these D-spreads were not able to reproduce the observed spectrum along the trigonal axis since none of the hyperfine signals in the $\pm 1/2 \leftrightarrow \pm 3/2$ transitions could be split in more than seven lines by the remaining terms in the operator.

The Cs_2MnF_6 spectra along the four- and 3-fold axis were *fitted* simultaneously with the exceedingly versatile program Efit[17] which operates through full diagonalization of the energy matrix at each field value and calculates a transition probability and a band shape. With a dimension of $(2S + 1)(2I_{Mn} + 1)(2I_F + 1)^6 = 1536$, however, the size of the matrix in the direct product basis was computationally prohibitive. This issue was overcome by changing to a coupled basis where the spins of opposite fluoride ligands were coupled. This transforms the energy matrix into a block diagonal form where each block could be diagonalized separately; the block dimensions are 648, 3×216, 3×72 and 24.

When fitting the cubic spectra the number of lines along the 3-fold axis could only be accounted for when $A_{F||}$ and $A_{F\perp}$ had different signs and because the nuclear Zeeman effect of fluorine is comparable in size to the superhyperfine coupling to fluorine. As will be explained later the fitting of the spectra of the trigonal distorted potassium salt gave the absolute signs of these fluoride superhyperfine parameters. Because of the great similarity between the two systems, the signs can be transferred from the trigonal to the cubic system leaving $A_{F||}$ negative and $A_{F\perp}$ positive. The sign of A_{Mn} could not be determined from the recorded spectra but was chosen to be negative in accordance with what has previously been determined for Mn(II).[17] The parameters accounting for all the lines in the cubic spectra are collected in Table 1. However, the spectra seemed to lack some intensity in the wings. Therefore the following higher order terms were included in the spin Hamiltonian:

$$u\left(\hat{S}_x^3 B_x + \hat{S}_y^3 B_y + \hat{S}_z^3 B_z - \frac{1}{5}(\hat{\mathbf{S}}\cdot\mathbf{B})(3\hat{\mathbf{S}}^2 - 1)\right)$$

$$U_{Mn}\left(\hat{S}_x^3 \hat{I}_{Mn,x} + \hat{S}_y^3 \hat{I}_{Mn,y} + \hat{S}_z^3 \hat{I}_{Mn,z} - \frac{1}{5}(\hat{\mathbf{S}}\cdot\hat{\mathbf{I}}_{Mn})(3\hat{\mathbf{S}}^2 - 1)\right)$$

$$U_F \sum_{i=1}^{6}\left(\hat{S}_x^3 \hat{I}_{F(i)x} + \hat{S}_y^3 \hat{I}_{F(i)y} + \hat{S}_z^3 \hat{I}_{F(i)z} - \frac{1}{5}(\hat{\mathbf{S}}\cdot\hat{\mathbf{I}}_{F(i)})(3\hat{\mathbf{S}}^2 - 1)\right)$$

The introduction of these parameters improves the fit significantly. The extra parameters were validated through an F-test giving 0. We did no attempt to validate the signs of these higher order terms and have just accepted the signs from the fittings: $u = 0.65(2) \times 10^{-4}$ cm^{-1}, $U_{Mn} = 0.103(2) \times 10^{-4}$ cm^{-1}, $U_F = -0.69(1) \times 10^{-4}$ cm^{-1}.

Fitting of K_2MnF_6. The allowed transitions in the spectra of K_2MnF_6 diluted in K_2GeF_6 recorded parallel and perpendicular to the 3-fold axis are depicted in Figures 3−7. Simplified energy level diagrams, excluding nuclear spins, can be seen in Figure 8 and 9. The major difference between the trigonal and the cubic spectrum is that the lower symmetry of the trigonal spectrum introduces a traditional zero field splitting which separates out the allowed transitions in M_S. This zero field splitting showed a temperature dependence of approximately 1.7% between 120 and 20 K. Additionally, the resolution of the superhyperfine lines seemed to drop when the temperature came below a certain point. Both effects are illustrated in Figure 10. The spectra were therefore recorded at 80 K as a compromise between superhyperfine resolution and signal-to-noise ratio.

(15) Cohen, E. R.; Cvitaš, T.; Frey, J. G.; Holmström, B.; Kuchitsu, K.; Marquardt, R.; Mills, I.; Pavese,F.; Quack, M.; Stohner, J.; Strauss, H. L.; Takami, M.; Thor, A. J. *Quantities, Units and Symbols in Physical Chemistry*; RSC Publishing: Cambridge, 2007.

(16) Davies, J. J.; Smith, S. R. P.; Owen, J.; Hann, B. F. *J. Phys. C: Solid Stat. Phys.* **1972**, *5*, 245–256.

(17) Piligkos, S.; Laursen, I.; Morgenstjerne, A.; Weihe, H. *Mol. Phys.* **2007**, *105*, 2025–2030.

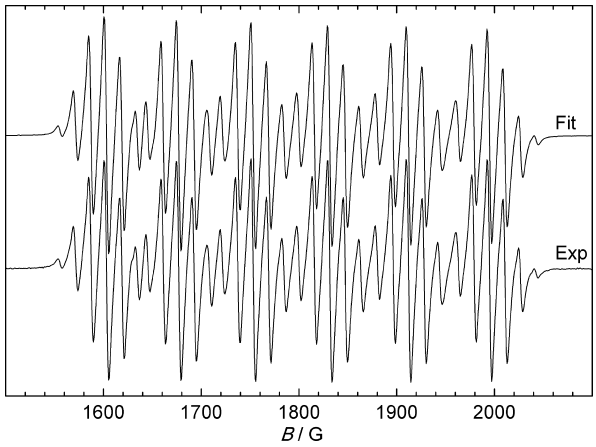

Figure 6. EPR spectrum showing the transition 1/2↔3/2 (high field labels) in diluted K_2MnF_6 recorded perpendicular to the 3-fold axis (cf. Figure 9F), $\nu = 9.6367$ GHz.

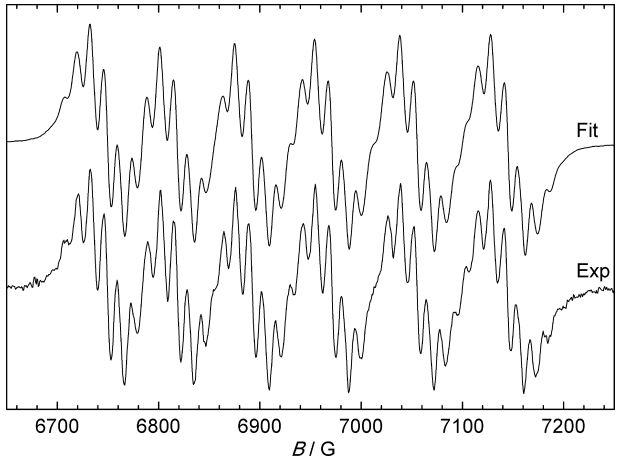

Figure 7. EPR spectrum showing the transition −3/2↔−1/2 (high field labels) in diluted K_2MnF_6 recorded perpendicular to the 3-fold axis (cf. Figure 9G), $\nu = 9.6367$ GHz.

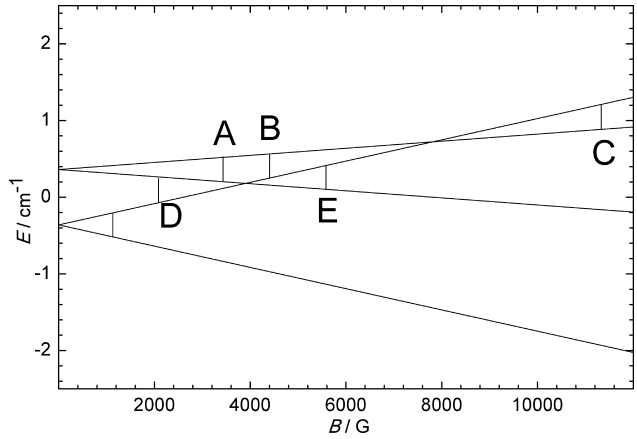

Figure 8. Field dependence of the energy levels in K_2MnF_6 along the 3-fold axis.

When fitting the trigonal spectrum, all the superhyperfine matrices were treated as if the fluoride ligands were placed in the corners of a regular octahedron. We thereby neglect any off-diagonal low symmetry components resulting from the trigonal distortion. The potassium spectra could be fitted with the following spin Hamiltonian:

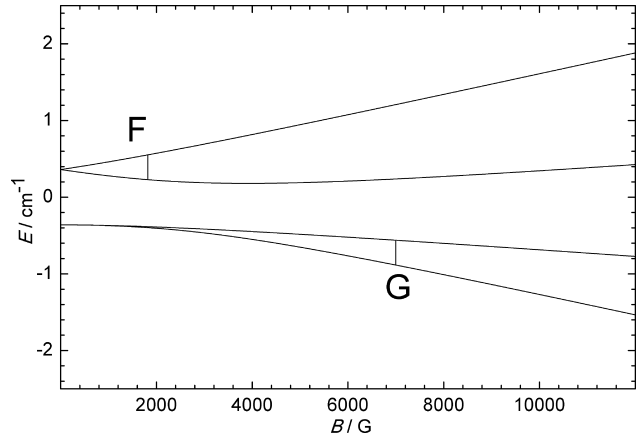

Figure 9. Field dependence of the energy levels in K_2MnF_6 perpendicular to the 3-fold axis.

$$\hat{H} = \mu_B \mathbf{B}^T \cdot \mathbf{g} \cdot \hat{\mathbf{S}} + \hat{\mathbf{S}}^T \cdot \mathbf{D} \cdot \hat{\mathbf{S}} + \hat{\mathbf{S}}^T \cdot \mathbf{A}_{Mn} \cdot \hat{\mathbf{I}}_{Mn} + \sum_{i=1}^{6} \hat{\mathbf{S}}^T \cdot \mathbf{A}_{F(i)} \cdot \hat{\mathbf{I}}_{F(i)} - \sum_{i=1}^{6} g_{N,F} \mu_N \mathbf{B}^T \cdot \hat{\mathbf{I}}_{F(i)} - g_{N,Mn} \mu_N \mathbf{B}^T \cdot \hat{\mathbf{I}}_{Mn}$$

The principal axes of the **g**-, $\mathbf{A}_{Mn}$-, and **D**-matrices are collinear with the trigonal distortion and therefore noncollinear with the principal axes of the superhyperfine matrices. The components $g_{||}$ and $g_{\perp}$, referred to the trigonal axis, should be almost equal because of the non-orbital degeneracy of the ground state. The same holds for $A_{Mn||}$ and $A_{Mn\perp}$. An approximate numerical value of A_{Mn} and D was estimated through simulations performed with a smaller basis leaving out the fluoride spins.

The sign of D was determined through high field measurements at 230 GHz on a diluted powder sample. This was done by observing the change in intensity of the different transitions as a response to temperature changes. As can be seen from Figure 11 the sign of D is negative. The size of D is similar to the value previously found by Flint et al.[18] measuring on Cs_2MnF_6 diluted in trigonal distorted Cs_2TiF_6. Their discussion, however, left some ambiguity about the sign. The powder simulations in Figure 11 were also performed with a smaller basis leaving out all nuclear spins.

To speed up the fitting procedure, the parallel and perpendicular crystal orientation were fitted independently, and instead of trying to determine a spread in D, each transition in M_S was allowed for a different bandwidth.

Knowing the sign of D also fixed the signs of $A_{F||}$ and $A_{F\perp}$; only a negative $A_{F||}$ and a positive $A_{F\perp}$ can reproduce the observed spectra. From the measurements, it was not possible to deduce the sign of A_{Mn} but, as in the cubic case, a negative sign was chosen. The extracted parameters are given in Table 1.

When the sample was cooled further it was possible to observe forbidden transitions $\Delta M_S = \pm 2$, $\Delta M_{I,Mn} = \mp 1$ along the trigonal axis (Figure 12 and 13). To increase the signal-

(18) Manson, N. B.; Shah, G. A.; Howes, B.; Flint, C. D. *Mol. Phys.* **1977**, *34*, 1157–1174.

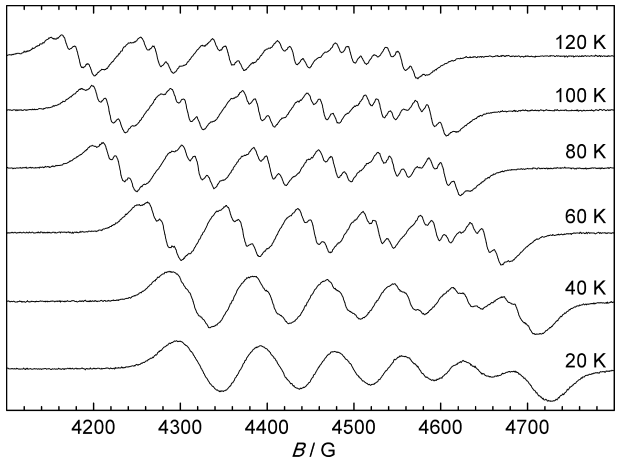

Figure 10. Temperature dependence of the transition 3/2↔1/2 in K_2MnF_6 recorded along the 3-fold axis (cf. Figure 8B), $\nu = 9.64$ GHz.

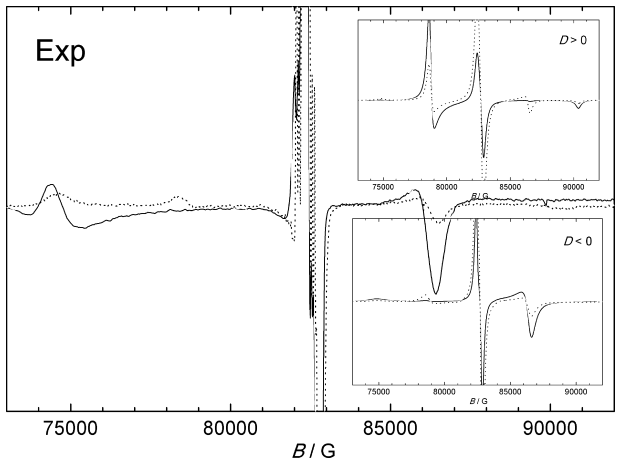

Figure 11. Temperature dependence of the EPR powder spectrum of K_2MnF_6 in K_2GeF_6 at 230 GHz. Black, 5 K, gray, 10 K, and dotted black, 25 K. The insets shows simulated temperature dependence using a positive (upper) and negative (lower) D-parameter. The spectra are simulated with the parameters $g = 1.99$, $|D| = 0.362$ cm^{-1} and a Gaussian D-spread $\sigma_D = 0.04$ cm^{-1}. Powder simulations were performed with the program Sim.[7]

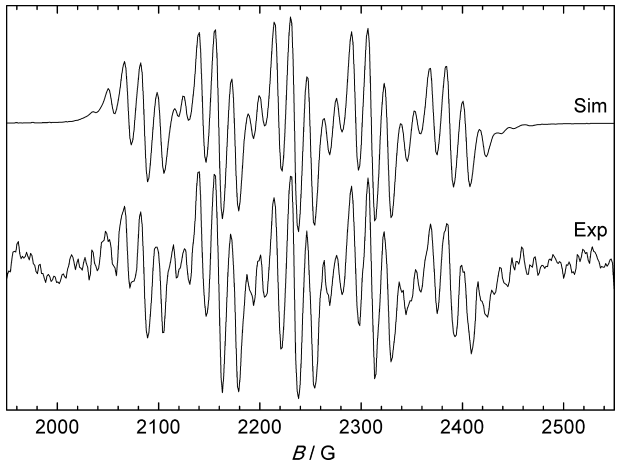

Figure 12. EPR spectrum showing the transition 3/2↔−1/2 in diluted K_2MnF_6 recorded along the 3-fold axis (cf. Figure 8D), $\nu = 9.637$ GHz.

to-noise ratio of these, the temperature was lowered to 25 K. These spectra could also be simulated with the hyperfine and superhyperfine parameters given in Table 1 when allowing for new bandwidths. It was, however, necessary to slightly modify the D-parameter because of its temperature dependence and the g-value because of an inaccuracy in orientation.

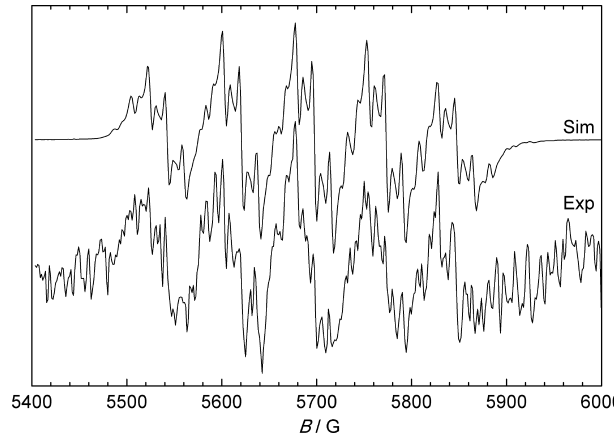

Figure 13. EPR spectrum showing the transition −1/2↔3/2 in diluted K_2MnF_6 recorded along the 3-fold axis (cf.Figure 8E), $\nu = 9.637$ GHz.

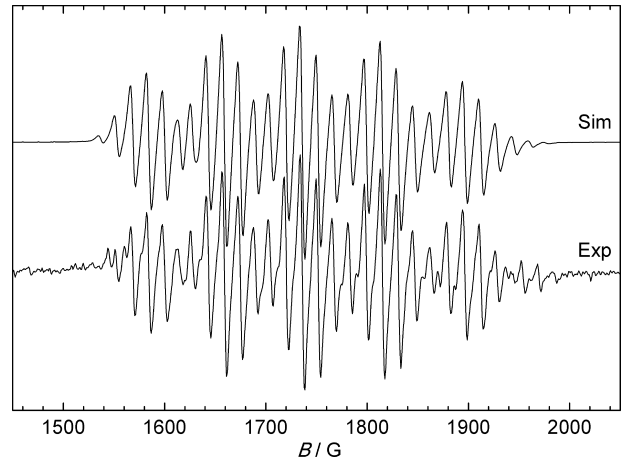

Figure 14. EPR spectrum showing the transition 1/2↔3/2 (high field labels) in diluted K_2MnF_6 recorded perpendicular to the 3-fold axis with parallel microwave polarization (cf. Figure 9F), $\nu = 9.4343$ GHz. The extra lines observed in the experimental spectrum are caused by microwave radiation, with wrong polarization, entering the cavity.

A low intensity spectrum perpendicular to the 3-fold axis was also observed when the microwave polarization was changed from perpendicular to parallel mode (Figure 14). The spectrum was recorded at 25 K to increase the signal-to-noise ratio. The spectrum could be simulated with the parameters given in Table 1 perpendicular to the 3-fold axis when small corrections in D and g were again allowed for. The parallel polarization spectrum shows a hyperfine quintet indicating a selection rule $\Delta M_{I,\mathrm{Mn}} = \pm 1$.

Discussion

Disappearance of the ±1/2↔±3/2 transitions in cubic systems has previously been observed in a number of d^3-systems.[16,19] The effect is a result of not all paramagnetic centers being in a totally cubic environment but instead suffering from small random trigonal distortions. The extent of these distortions may depend on the size-match between the paramagnetic ion and the host.

Our superhyperfine parameters for Cs_2MnF_6 are similar to parameters previously found by a theoretical paper.[20] For

(19) Rahn, R. O.; Dorain, P. B. *J. Chem. Phys.* **1964**, *41*, 3249–3254.

Table 2. Superhyperfine (Unit 10^{-4} cm^{-1}) Data for Selected d^3 Systems from the First Transition Period[a]

ion	R/Å	g	$A_{F\|\|}$	$A_{F\perp}$	A_s	A_a	A_d	A_π	A_σ	ref
VF_6^{4-}	1.995	1.972	−7.002	−1.90	−3.60	−1.70	3.1	4.8	0	16
CrF_6^{3-}	1.885	1.974	−9.34	2.71	−1.31	−4.01	3.7	7.7	0	22
MnF_6^{2-}	1.794	1.988	−16.76	13.55	3.45	−10.10	4.3	14.4	0	

[a] Distances are taken from the hosts.

orbital non-degenerate octahedral systems superhyperfine parameters are traditionally separated into an isotropic part A_s and an anisotropic part A_a:[2,21]

$$A_{||} = A_s + 2A_a$$

$$A_\perp = A_s - A_a$$

The anisotropic part consists of a dipolar contribution A_d, a π contribution A_π and a σ contribution A_σ:

$$A_a = A_d + A_\sigma - A_\pi$$

Because d^3 systems in octahedral symmetry do not have any e_g electrons, A_σ should be zero. A_d can be calculated from the formula:

$$A_d = \frac{\mu_0 g \mu_B g_{N,F} \mu_N}{4\pi R^3} = 4.3 \times 10^{-4}\ cm^{-1}$$

where $R = 1.794$ Å is taken from the host.

Knowing A_d it is possible to calculate A_π. In Table 2 A_π is compared to similar data for the isoelectronic systems VF_6^{4-} [16] and CrF_6^{3-}.[22] The π-parameters clearly reflect how the increased charge on the metal center attracts electron density from the fluoride ligands leading to an increase in A_π.

A_s represents a Fermi contact interaction due to σ-overlap between e_g orbitals on the metal ion and s orbitals on the fluoride ions. As already mentioned, there are no unpaired e_g electrons in octahedral d^3 systems, yet, A_s differs slightly from zero. The reason for this is unclear, but small deviations from zero are also seen for the other d^3 systems in Table 2.

For axially elongated MnF_6^{3-} it has recently been found that A_s gives the main contribution to the superhyperfine parameters.[23] The parameter is roughly around 40×10^{-4} cm^{-1}. This is much larger than the A_s parameters obtained for d^3 systems and consistent with the manganese(III) system having one unpaired e_g electron.

The parameters obtained from the cubic and hexagonal system are nearly equivalent in accordance with the great similarity between the two systems. The fittings completely reproduce the experimental spectra. It shows that the approximation made when treating the distorted fluoride ligands as if they were placed in a regular octahedron is a decent one. The discrepancy between the parameters for the hexagonal system obtained parallel and perpendicular to the unique axis is most likely due to a diminutive inaccuracy in the crystal alignment.

Acknowledgment. The authors wish to thank Dr. Høgni Weihe for providing the simulation and fitting software.

IC802223J

(20) Wu, S.-Y.; Gao, X.-Y.; Dong, H.-N. *Z. Naturforsch., A: Phys. Sci.* **2005**, *60*, 611–614.

(21) Hall, T. P. P.; Hayes, W.; Stevenson, R. W. H.; Wilkens, J. *J. Chem. Phys.* **1963**, *38*, 1977–1984.

(22) We have extracted these parameters through fitting of EPR spectra of cubic, elpasolite type, single crystals of K_2NaCrF_6 diluted in K_2NaGaF_6. Signs of the parameters are taken from Vrielinck, H.; Loncke, F.; Callens, F.; Matthys, P.; Khaidukov, N. M. *Phys. Rev. B: Condens. Matter* **2004**, *70*, 144111; The Ga-F distance has been determined through single crystal X-ray measurements.

(23) Scheifele, Q.; Birk, T.; Bendix, J.; Tregenna-Piggott, P. L. W.; Weihe, H. *Angew. Chem., Int. Ed.* **2008**, *47*, 148–150.